Physics of the Earth and Planetary Interiors 245 (2015) 71–75

Contents lists available at ScienceDirect

Physics of the Earth and Planetary Interiors

journal homepage: www.elsevier.com/locate/pepi

Letter

A regional test of global models for flow, rheology, and seismic anisotropy at the base of the mantle

Heather A. Ford *, Maureen D. Long

Department of Geology and Geophysics, Yale University, PO Box 208109, New Haven, CT 06520-8109, USA

ARTICLE INFO

Article history:
Received 18 March 2015
Received in revised form 24 April 2015
Accepted 11 May 2015
Available online 27 May 2015

Keywords:
Anisotropy
Shear wave splitting
Global lowermost mantle flow models

ABSTRACT

The study of flow patterns and seismic anisotropy in the lowermost mantle is fraught with uncertainties, given the limitations in our understanding of the physical properties of the lowermost mantle and the relationships between deformation and anisotropy. Here we use a set of SKS, SKKS, and ScS splitting measurements that sample the eastern edge of the African Large Low Shear Velocity Province to test predictions of seismic anisotropy derived from previously published 3D global mantle flow models and anisotropy modeling (Walker et al., 2011). The observations can be fit by a model that invokes flow directed to the southwest with a component of downwelling in our study region, and slip that occurs along the (010) plane of post-perovskite. Most importantly, we demonstrate the ability of a regional shear wave splitting data set to test the robustness of models for flow and deformation in the lowermost mantle.

1. Introduction

Global models of radial anisotropy (e.g., Kustowski et al., 2008; Panning et al., 2010) and regional body wave data sets (e.g., Nowacki et al., 2010; Cottaar and Romanowicz, 2013) indicate that the lowermost mantle is seismically anisotropic, in contrast to the rest of the (predominantly) isotropic lower mantle. Observations of anisotropy in the lowermost mantle (the D″ layer) are plentiful and robust, but the mechanism for anisotropy is debated, with both shape preferred orientation (SPO) and lattice preferred orientation (LPO) scenarios possible. Most studies focus on the LPO of phases such as MgO (e.g., Wenk et al., 2011) and/or post-perovskite (e.g., Nowacki et al., 2010; Ford et al., 2015).

Single-crystal elasticity and texture development remain to be elucidated in full for lower mantle materials, and the composition and mineralogy remains uncertain (e.g., Cobden et al., 2012; Grocholski et al., 2012). Despite these limitations, a promising approach for investigating lowermost mantle flow is to carry out global flow models based on density structures inferred from tomography (Simmons et al., 2007, 2009). If reasonable assumptions about elasticity and LPO are made, such models can make testable predictions about the geometry of anisotropy in the lowermost mantle that can be compared against observations of D″ anisotropy. Using global radial anisotropy models, Walker et al. (2011) tested the predictions made by such flow models and suggested that regional body-wave datasets could serve as a useful additional test.

Here we carry out such a test using a previously published set of shear wave splitting measurements that sample the lowermost mantle beneath the Afar region of Africa (Fig. 1). Our study region lies just outside the eastern edge of the African Large Low Shear Velocity Province (LLSVP) and is sampled by SKS, SKKS, and ScS raypaths propagating at five distinct orientations, allowing for a careful comparison between flow model predictions and shear wave splitting observations. We test the predictions of lowermost mantle elasticity made by Walker et al. (2011) derived from a suite of numerical flow models assuming dislocation creep in a post-perovskite aggregate.

2. Methods

2.1. Shear wave splitting data set

The data set used in this study is described in detail in Ford et al. (2015) and comprises 22 shear wave splitting measurements for SKS, SKKS and ScS phases recorded at 9 stations in Africa and Europe, corrected for upper mantle anisotropy and averaged into five groups according to their raypath propagation direction (Fig. 1 and Tables S1 and S2). We obtained results for two sets of ScS paths, two sets of SKKS paths, and one set of SKS paths. We observed splitting behavior that was consistent within each raypath-averaged group of measurements (Ford et al., 2015) but

* Corresponding author.
E-mail address: heather.ford@yale.edu (H.A. Ford).

http://dx.doi.org/10.1016/j.pepi.2015.05.004
0031-9201/

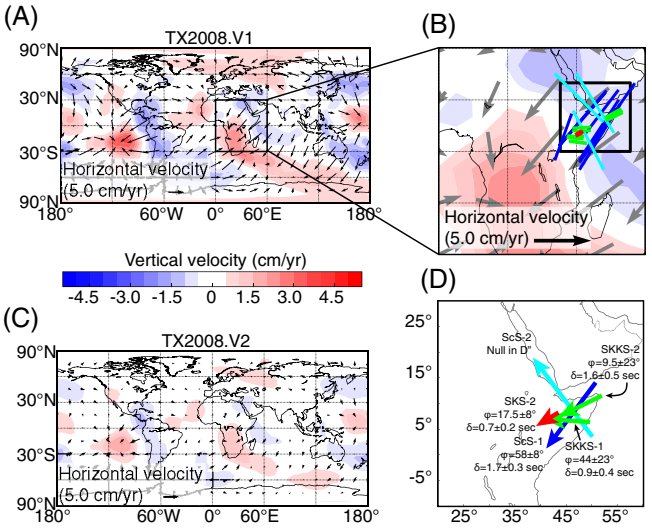

Fig. 1. (A) Map of horizontal (arrows) and vertical (colors) mantle flow at a depth 150 km above the CMB, for flow model TX2008.V1. Modified from Walker et al. (2011). (B) Flow model TX2008.V1 in our study region. Black square indicates region over which we average elastic constants. Colored lines indicate sampling of the D″ region by the body wave phases used in this study (from Ford et al., 2015). Portions of ray paths sampling the bottom 250 km of mantle are shown for ScS (blue and cyan), SKKS (green) and SKS (red). (C) Same as (A) for flow model TX2008.V2. (D) Schematic of raypath-averaged splitting parameters. Arrows correspond to the average raypaths of ScS (blue, cyan), SKKS (green) and SKS (red) through bottom 250 km of mantle. SKS and SKKS path lengths are exaggerated (2×) for clarity. (For interpretation of the references to color in this figure legend, the reader is referred to the web version of this article.)

varied with direction, suggesting anisotropy that deviates from vertical transverse isotropy (VTI).

2.2. Mantle flow and elasticity models

The instantaneous global flow models calculated by Walker et al. (2011) form the basis of our predictions. The modeled mantle velocities result from viscous flow modeling (e.g., Forte, 2007) that relies on the joint inversion of seismic and geodynamic data. For each set of model mantle flow velocities, Walker et al. (2011) computed the texture evolution of a post-perovskite aggregate from a visco-plastic self-consistent approach (Lebensohn and Tomé, 1993), producing calculated elastic stiffness tensors throughout the lowermost mantle. An important aspect of this modeling is the assumption that seismic anisotropy is the result of LPO development dominated by slip along either the (001), (010), or (100) planes of post-perovskite.

The flow models that we tested assume one of two one-dimensional mantle viscosity models (Mitrovica and Forte, 2004) and one of two of mantle density models derived from the tomographic inversion of seismic and geodynamic observations (Simmons et al., 2007, 2009). Following Walker et al. (2011), we refer to the calculated flow models (and their corresponding elastic constants) according to the particular density (TX2007, TX2008; Simmons et al., 2007, 2009) and viscosity (V1, V2; Mitrovica and Forte, 2004) model used to produce the velocity field. The TX2008 density model is generally smoother than TX2007, and V2 has generally higher viscosities than V1 (Fig. 1). In the flow models the bridgmanite to post-perovskite phase transition was generally set to a constant depth of 150 km above the CMB, implying a lack of temperature dependence. However, we also considered a set of cases for TX2008.V2 in which the phase transition depended on both temperature and pressure, producing topography on the boundary (referred to as TX2008.V2T). As with all global models of mantle flow, these models make a number of assumptions; caveats associated with viscous flow modeling are discussed by Zhong et al. (2007).

2.3. Shear wave splitting predictions and comparisons

We approximate the elasticity over the region sampled by our observations (Fig. 1) by computing a linear average for each elastic constant over 0–20°N in latitude and 35–55°E in longitude for each set of model elastic constants (Fig. 2). This averaging scheme is appropriate given the modest changes in flow velocities and radial anisotropy predicted across our study region (Fig. 1). Fig. 2 shows splitting predictions for the spatially averaged elasticity model for TX2008.V1 (assuming slip on the (010) plane) along with predictions derived from elasticity tensors for individual model points. Changes in the modeled elastic tensor within our study region are modest, demonstrating that our spatial averaging scheme represents the model elasticity well.

Using the spatially averaged elastic tensors for each model, we used MSAT (Walker and Wookey, 2012) to perform a ray theoretical prediction of the splitting parameters (ϕ, δt) for each of the five raypath directions in our data set. We also tested anisotropic geometries that are similar, but not identical, to those predicted by Walker et al. (2011) by varying the orientation of the elastic tensor up to 20° from the model prediction. These adjustments do not account for uncertainties in the flow model per se, since variations in model flow velocities would result in changes to the form of the elastic tensor itself beyond that of a simple rotation.

Residual sum of squares misfits between the predicted and observed S-wave fast polarization directions (ϕ) were calculated as described in Ford et al. (2015). Any model in which the misfit between the predicted and observed ϕ values exceeded 20° was discarded. After this initial culling of models, we predicted delay times (δt) for each raypath for the remaining candidate models. Because δt is a function of anisotropy strength and path length, we varied the thickness of the anisotropic layer (in 25 km increments) from 25 to 500 km, to test what layer thicknesses are consistent with the observations. For each model, we evaluated whether the difference between the predicted and observed δt exceeded a set threshold (0.75, 1, 1.25, or 1.5 s, which represent increasingly conservative estimates for the maximum errors on estimated delay times) for any given raypath-averaged observation; if so, that candidate model was discarded.

3. Results

We calculated predicted splitting parameters for 15 different sets of spatially averaged elastic tensors over a range of anisotropic layer thicknesses (25–500 km). For the initial cases in which tensor orientations were not allowed to vary, and misfits were limited to a maximum of 1 s in δt and 20° in ϕ for each raypath direction, we identified no flow model/slip plane combinations that reproduced the splitting observations. If the maximum allowable delay time misfit was increased to 1.25 or 1.5 s, a limited subset of cases was able to reproduce splitting results without having to be rotated. This suggests that the global flow models and/or our understanding of texture formation in post-perovskite are not a strictly accurate representation of the state of the lowermost mantle, at least in our study region.

For the second set of model comparisons, in which we allowed the orientation of the elastic tensor to be rotated around each geographic axis by up to 20°, we found cases that reproduce our observations within the allowable misfit range (Table 1). We note that there is no case for which all δt misfits are found to fit below the 0.75 s threshold, even allowing for rotations of the elastic tensor.

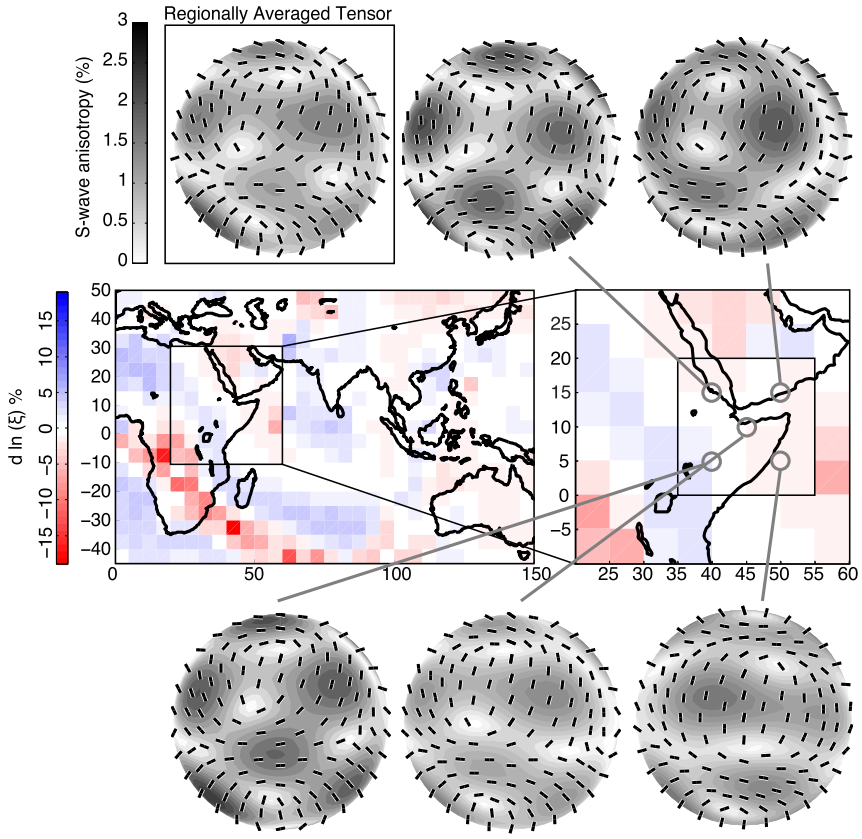

Fig. 2. Elasticity and anisotropy of the lowermost mantle in our study region predicted by flow model TX2008.V1 with slip plane (010), from Walker et al. (2011). Maps in middle panels illustrate radial shear wave anisotropy $\left(\xi = \frac{V_{SH}^2}{V_{SV}^2}\right)$. Stereoplots above and below the maps show upper hemisphere pole figures of predicted shear wave splitting behavior (fast shear wave polarization direction and S-wave anisotropy strength) for selected points within our study region, as indicated on the map. Stereoplot in the upper left-hand corner shows splitting predictions for the spatially averaged elastic tensor; the averaging region is shown as the black square in the map to the right.

Table 1
Summary of models whose predicted polarizations (ϕ) and delay times (δt) fall within the range of permissible misfit values. Acceptable thicknesses of the anisotropic layer (H) are given as a range for each model. Color corresponds to the maximum allowable δt misfit for any given observation.

		Slip Plane		
		(001)	(010)	(100)
Flow Model	TX2007.V1			
	TX2007.V2			H =25 km
	TX2008.V1		H=100-275 km H=25-300 km	
	TX2008.V2		H=200-375 km H=100-425 km H=25-475 km	
	TX2008.V2T			H =25 km

KEY
dt misfits of up to 1 sec
dt misfits of up to 1.25 sec
dt misfits of up to 1.5 sec

A striking observation is that among model cases that fit the observations, scenarios in which deformation is accommodated via slip on the (010) plane are heavily favored. When maximum delay time misfits are limited to 1 or 1.25 s, the only elastic constant models for which we find an acceptable match are those for which slip occurs along (010). The acceptable models include TX2008.V1 and TX2008.V2, over a large range of anisotropic layer thicknesses (Table 1). If the δt misfit threshold is increased to 1.5 s, two additional sets of elastic constants, corresponding to TX2007.V2 and TX2008.V2T deformed along the (100) slip plane, are permitted. However, in both cases the thickness of the anisotropic layer cannot exceed 25 km without overpredicting some delay times. While a thin layer of anisotropy is plausible in regions of elevated temperatures, the fact that the acceptable models require a small range of permissible layer thicknesses while allowing for very large delay time uncertainties suggests that these scenarios are less likely.

Other than these two model outliers, the remaining models that fit the observations invoke the smoother density model (TX2008) along with slip on the (010) plane (Table 1). Either viscosity model provides an acceptable fit to the observations for this scenario; a reasonable range of acceptable layer thicknesses is identified, typically ~100–400 km. Splitting predictions for the two elasticity models we favor (TX2008.V1 and TX2008.V2) are shown in Fig. 3, which shows predicted and observed polarization directions and predicted anisotropy strength for a range of propagation directions.

4. Discussion

4.1. Implications for deformation and anisotropy mechanisms

Our results reveal important insights about likely deformation mechanisms in the lowermost mantle. First, the fact that we can identify elasticity models that are similar (with small rotational

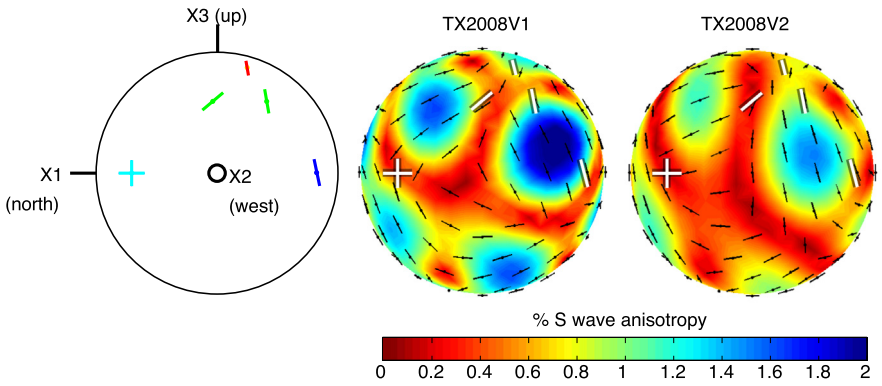

Fig. 3. (Left) Spherical projection of raypath-averaged ϕ observations for ScS (blue and cyan), SKKS (green) and SKS (red) phases in the shear wave splitting data set, ScS null (cyan) is shown as perpendicular cross hairs, which correspond to the calculated polarization direction (and its orthogonal direction) of the incoming ScS wave; details are described in Ford et al. (2015). (Middle and right) Shear wave splitting predictions (thin black lines) and observations (white lines) for averaged and rotated elastic constants for TX2008.V1 and TX2008.V2. Each plot represents a spherical projection for all possible wave propagation directions; colors denote predicted anisotropy strength. (For interpretation of the references to color in this figure legend, the reader is referred to the web version of this article.)

adjustments) to those predicted by the Walker et al. (2011) models suggests that the LPO of post-perovskite deformed via dislocation creep is a plausible explanation for our observations. This inference is useful in light of lingering uncertainties over the dominant mineralogical phase(s) in the lowermost mantle (e.g., Grocholski et al., 2012) and the dominant mechanism(s) for seismic anisotropy.

Another implication comes from the finding that the models that provide the most robust fits to the observations (Fig. 3) invoke deformation that is accommodated via slip along the (010) plane. A similar study by Nowacki et al. (2013) that tested the predictions of the same elasticity models against an ScS splitting dataset beneath North America also identified slip on (010) as the most likely scenario. Likewise, Walker et al. (2011) suggested that slip occurring on (100) or (010) is most consistent with global radial anisotropy models. In contrast, Wenk et al. (2011) compared 2D flow models of a subducting slab to radial anisotropy models (Panning and Romanowicz, 2006) and concluded that anisotropy in paleoslab regions is best explained by (001) slip in post-perovskite. A follow-up study by Cottaar et al. (2014) using 3D models came to a similar conclusion, favoring post-perovskite slip on the (001) plane.

4.2. Implications for mantle flow

The two flow models (TX2008.V1 and TX2008.V2) that successfully match our observations involve similar flow geometries in our study region, with predominantly horizontal flow directed to the southwest and a slight downwelling component (Fig. 1). We reiterate, however, that the elasticity tensors directly predicted by these flow models are not generally consistent with the splitting dataset; it is only when the orientation of the elastic tensor is adjusted slightly via rotation that an acceptable fit to the data is achieved. We note further that the flow models of Walker et al. (2011) do not generally predict strong deformation, and thus anisotropy, along the edge of the African LLSVP, which has been inferred from recent observations (Wang and Wen, 2007; Cottaar and Romanowicz, 2013; Lynner and Long, 2014). This may suggest that dynamic processes are operating at the edges of LLSVPs that are not captured by the global mantle flow models.

The southwest-directed horizontal flow with a modest downwelling component that we identified as plausible in this study contrasts with results we obtained recently using the same splitting dataset but a different modeling approach, focusing on single-crystal elastic tensors. Our previous work (Ford et al., 2015) evaluated elasticity models based on single-crystal anisotropy of post-perovskite (among other minerals, which were not found to be compatible with observations). Within that framework, we identified flow with a significant upwelling component, resulting in a [100] axis of post-perovskite oriented either nearly vertically or oblique to the horizontal, as most consistent with the data. Another difference between the two modeling approaches is the treatment of the relationship between deformation and LPO. In our previous work, we assumed that [100] was the most likely slip direction based on experiments with analog materials (e.g., Miyagi et al., 2008) and further assumed that this direction is oriented parallel to the shear direction, as is generally the case for dislocation creep (Karato, 2008).

Given the uncertainties that remain in our understanding of LPO development in the lowermost mantle, both the approach taken in Ford et al. (2015) and the approach taken in this study and by Walker et al. (2011) are justifiable. The significantly different plausible flow scenarios identified in this study and by Ford et al. (2015) highlight the limitations in our knowledge of the elasticity and deformation of post-perovskite and the need for further study of lowermost mantle anisotropy using the tools of mineral physics, geodynamics, and seismology.

5. Conclusions

This paper presents a case study in testing the validity of 3D mantle flow model predictions (and their assumptions) using regional observations of lowermost mantle anisotropy. We tested the predictions of a set of global models of mantle flow and elasticity (Walker et al., 2011) against a shear wave splitting dataset that samples the lowermost mantle beneath Africa. We identified model cases that are consistent with observations, although slight modifications of the elastic tensor via rotation were needed to fit the data. Our observations favor models that rely on the TX2008 density model and invoke deformation of post-perovskite via slip on the (010) plane. Uncertainties associated with the composition, mineralogy and deformation of lowermost mantle minerals, as well as uncertainties in the tomography models themselves, mean that inferences about plausible mantle flow directions are non-unique. Additionally, while we were able to identify models that fit the data, it is possible that this conclusion is regionally specific; further study with larger data sets is needed to validate such flow models globally. Despite this, we have demonstrated the ability of regional shear-wave splitting data to test the predictions of global models for flow in the lowermost mantle.

Acknowledgments

We are grateful to Shun Karato for discussions about elasticity and deformation of lower mantle minerals and to Andrew Walker for making the elastic constants used in this study publicly available. We thank editor George Helffrich and an anonymous reviewer for constructive comments that helped to improve this paper. This work was supported via NSF grant EAR-1150722.

Appendix A. Supplementary data

Supplementary data associated with this article can be found, in the online version, at http://dx.doi.org/10.1016/j.pepi.2015.05.004.

References

Cobden, L., Mosca, I., Trampert, J., Ritsema, J., 2012. On the likelihood of post-perovskite near the core–mantle boundary: a statistical interpretation of seismic observations. Phys. Earth Planet. Inter. 210, 21–35.

Cottaar, S., Li, M., McNamara, A.K., Romanowicz, B., Wenk, H.R., 2014. Synthetic seismic anisotropy models within a slab impinging on the core–mantle boundary. Geophys. J. Int. 199, 164–177.

Cottaar, S., Romanowicz, B.A., 2013. Observations of changing anisotropy across the southern margin of the African LLSVP. Geophys. J. Int. 195, 1184–1195.

Ford, H.A., Long, M.D., He, X., Lynner, C., 2015. Lowermost mantle flow at the eastern edge of the African Large Low Shear Velocity Province. Earth Planet. Sci. Lett. 420, 12–22.

Forte, A. M., 2007. Constraints on seismic models from other disciplines – implications for mantle dynamics and composition. In: Romanowicz, B. and Dziewonski, A. (Eds.), Treatise on Geophysics. Seismology and the Structure of the Earth, vol. 1. Elsevier, Amsterdam, pp. 805–858. doi: http://dx.doi.org/10.1016/B978- 044452748-6.00027-4.

Grocholski, B., Catalli, K., Shim, S.-H., Prakapenka, V., 2012. Mineralogical effects on the detectability of the postperovskite boundary. Proc. Natl. Acad. Sci. 109, 2275–2279.

Karato, S.-I., 2008. Deformation of Earth Materials: An Introduction to the Rheology of Solid Earth. Cambridge University Press, Cambridge, UK.

Kustowski, B., Ekström, G., Dziewoński, A.M., 2008. Anisotropic shear-wave velocity structure of the Earth's mantle: a global model. J. Geophys. Res. 113, B06306. http://dx.doi.org/10.1029/2007JB005169.

Lebensohn, R.A., Tomé, C.N., 1993. A self-consistent anisotropic approach for the simulation of plastic deformation and texture development of polycrystals: application to zirconium alloys. Acta Metall. Mater. 41, 2611–2624. http://dx.doi.org/10.1016/0956-7151(93)90130-K.

Lynner, C., Long, M.D., 2014. Lowermost mantle anisotropy and deformation along the boundary of the African LLSVP. Geophys. Res. Lett. 41 (3447–3454), 2014G. http://dx.doi.org/10.1002/L059875.

Mitrovica, J.X., Forte, A.M., 2004. A new inference of mantle viscosity based upon joint inversion of convection and glacial isostatic adjustment data. Earth Planet. Sci. Lett. 225, 177–189.

Miyagi, L., Nishlyama, N., Wang, Y., Kubo, A., West, D.V., Cava, R.J., Duffy, T.S., Wenk, H.R., 2008. Deformation and texture development in CaIrO3 post-perovskite phase up to 6 GPa and 1300 K. Earth Planet. Sci. Lett. 268, 515–525.

Nowacki, A., Walker, A.M., Wookey, J., Kendall, J.M., 2013. Evaluating post-perovskite as a cause of D′′ anisotropy in regions of palaeosubduction. Geophys. J. Int. 192, 1085–1090.

Nowacki, A., Wookey, J., Kendall, J.-M., 2010. Deformation of the lowermost mantle from seismic anisotropy. Nature 467, 1091–1094.

Panning, M.P., Lekić, V., Romanowicz, B.A., 2010. Importance of crustal corrections in the development of a new global model of radial anisotropy. J. Geophys. Res. 115, B12325. http://dx.doi.org/10.1029/2010JB007520.

Panning, M., Romanowicz, B., 2006. A three-dimensional radially anisotropic model of shear velocity in the whole mantle. Geophys. J. Int. 167, 361–379.

Simmons, N.A., Forte, A.M., Grand, S.P., 2007. Thermochemical structure and dynamics of the African superplume. Geophys. Res. Lett. 34, L02301. http://dx.doi.org/10.1029/2006GL028009.

Simmons, N.A., Forte, A.M., Grand, S.P., 2009. Joint seismic, geodynamic and mineral physical constraints on three-dimensional mantle heterogeneity: implications for the relative importance of thermal versus compositional heterogeneity. Geophys. J. Int. 177, 1284–1304.

Walker, A.M., Forte, A.M., Wookey, J., Nowacki, A., Kendall, J.-M., 2011. Elastic anisotropy of D″ predicted from global models of mantle flow. Geochem. Geophys. Geosyst. 12, Q10006. http://dx.doi.org/10.1029/2011GC003732.

Walker, A.M., Wookey, J., 2012. MSAT—a new toolkit for the analysis of elastic and seismic anisotropy. Comput. Geosci. 49, 81–90.

Wang, Y., Wen, L., 2007. Complex seismic anisotropy at the border of a very low velocity province at the base of the Earth's mantle. J. Geophys. Res. 112 (B09305), 2006J. http://dx.doi.org/10.1029/B004719.

Wenk, H.-R., Cottaar, S., Tomé, C.N., McNamara, A., Romanowicz, B., 2011. Deformation in the lowermost mantle: from polycrystal plasticity to seismic anisotropy. Earth Planet. Sci. Lett. 306, 33–45.

Zhong, S., Yuen, D.A., Moresi, L.N., 2007. Numerical methods for mantle convection. Treatise Geophys. 7, 227–252.